PNAS RESEARCH ARTICLE | EARTH, ATMOSPHERIC, AND PLANETARY SCIENCES

Temperature controls the episodic dynamics of deep slow slip

Zaccaria El Yousfi[a,1], Baptiste Rousset[b,2], Mathilde Radiguet[a], and William B. Frank[c,2]

Affiliations are included on p. 7.

Edited by Michael Manga, University of California, Berkeley, CA; received September 5, 2025; accepted March 10, 2026

The deformation regime that accommodates tectonic motion at plate boundaries changes as pressures and temperatures increase with depth, transitioning from the shallow frictional sliding of seismic ruptures to deep, viscous flow. We use recurring swarms of low-frequency earthquakes in this transition zone to measure the recurrence intervals and durations of accompanying slow slip across four plate boundaries. We find these time scales systematically decrease with depth and linearly scale with one another. Assuming a transition zone governed by episodic faulting, the observed time scales produce an average slow slip rate of 7 ± 2 mm/d across all four plate boundaries that is independent of depth. Thermal models place these slow slip dynamics within a common, narrow range of temperatures. Our results suggest deep slow slip is the result of the episodic unjamming of the plate boundary by frictional heterogeneities whose relaxation is modulated by surrounding temperature-dependent viscous material.

slow slip | low-frequency earthquakes | frictional–viscous transition

Significance

Episodic slow slip at the root of tectonic plate boundaries is a common mechanism by which plate motion is accommodated within the transition between shallow frictional earthquake slip and deep viscous creep. We use swarms of low-frequency earthquakes—tiny earthquakes that act as a proxy for fault motion within this frictional–viscous transition—to measure the duration and recurrence intervals of deep slow slip. The observed time scales of episodic faulting decrease with depth and imply the rate of slow slip is constant across four different tectonic plate boundaries. Thermal models of plate boundaries reveal a common temperature range for these dynamics, suggesting that temperature is the principal factor governing deep slow slip behavior across diverse tectonic environments.

The mode of deformation along tectonic plate boundary faults depends on pressure and temperature that both increase with depth (1). Within the shallow seismogenic zone (depths <30 km), deformation is governed by frictional instabilities sensitive to pressure, and episodic earthquakes dominate fault motion. At greater depths, the primary deformation mechanism along plate boundaries transitions to viscous flow with increasing temperatures. This transition not only represents changes in the dynamics of deformation (episodic to quasi-continuous motion) but also in the principal parameter that controls the mechanism (pressure to temperature). Geological observations of exhumed plate boundaries suggest that deformation within this transition zone results from an interplay of the end-member frictional and viscous regimes (2–4). Because this transition is not abrupt and likely plays out across some finite distance along the plate boundary, the relative partitioning of this frictional–viscous interplay should evolve with depth and depend on local temperature and pressure conditions.

Geodetic measurements of surface motion regularly image discrete episodes of fault slip too slow to radiate seismically within this transition zone at a number of plate boundaries, including subduction zones such as Nankai (5), Cascadia (6), Guerrero (7), Hikurangi (8), as well as transform plate boundaries like the Parkfield section of the San Andreas fault (9) and the North Anatolian fault (10, 11). Modeled as transient shear slip, slow slip events can last from hours to years, recur over the same range of time scales, and potentially release as much tectonic strain as a magnitude 7 earthquake (8, 12). While slow slip can also occur at shallow depths (<15 km) (11, 13, 14), we focus here on deep slow slip that samples the frictional–viscous transition downdip of the seismogenic zone. Within this deep transition zone, the presence of fluids from metamorphic dehydration of the subducting slab (4) allows for shear slip at depths below the seismogenic zone (15) by elevating pore pressures (16, 17). Both fluids (18) and viscous deformation (19, 20) have been proposed to keep deep slow slip slow, limiting the average speed of slow fault slip to subseismic slip rates.

Although the energy release of slow slip is overwhelmingly aseismic, colocated swarms of tiny repeating earthquakes on the plate boundary called low-frequency earthquakes can function as a seismic proxy for slow slip (21, 22). Slow slip is thought to rapidly load and trigger these seismic sources (23), generating many events from localized low-frequency earthquake sources (24). The timing of these swarms of repetitive seismic events provides a precise lens through which we can image slow slip dynamics with high temporal resolution (25–28).

The behavior of low-frequency earthquakes, and by proxy slow slip, varies systematically with depth (29–33). Close beneath the seismogenic zone, swarms of low-frequency earthquakes occur periodically and signal discrete episodes of slow slip (34, 35). At greater

Author contributions: Z.E.Y., B.R., and W.B.F. designed research; Z.E.Y., B.R., M.R., and W.B.F. performed research; Z.E.Y. and W.B.F. analyzed data; and Z.E.Y., B.R., M.R., and W.B.F. wrote the paper.

The authors declare no competing interest.

This article is a PNAS Direct Submission.

[1]To whom correspondence may be addressed. Email: zaccaria.el-yousfi@univ-grenoble-alpes.fr.

[2]B.R. and W.B.F. contributed equally to this work.

This article contains supporting information online at https://www.pnas.org/lookup/suppl/doi:10.1073/pnas.2524741123/-/DCSupplemental.

Published XXXX.

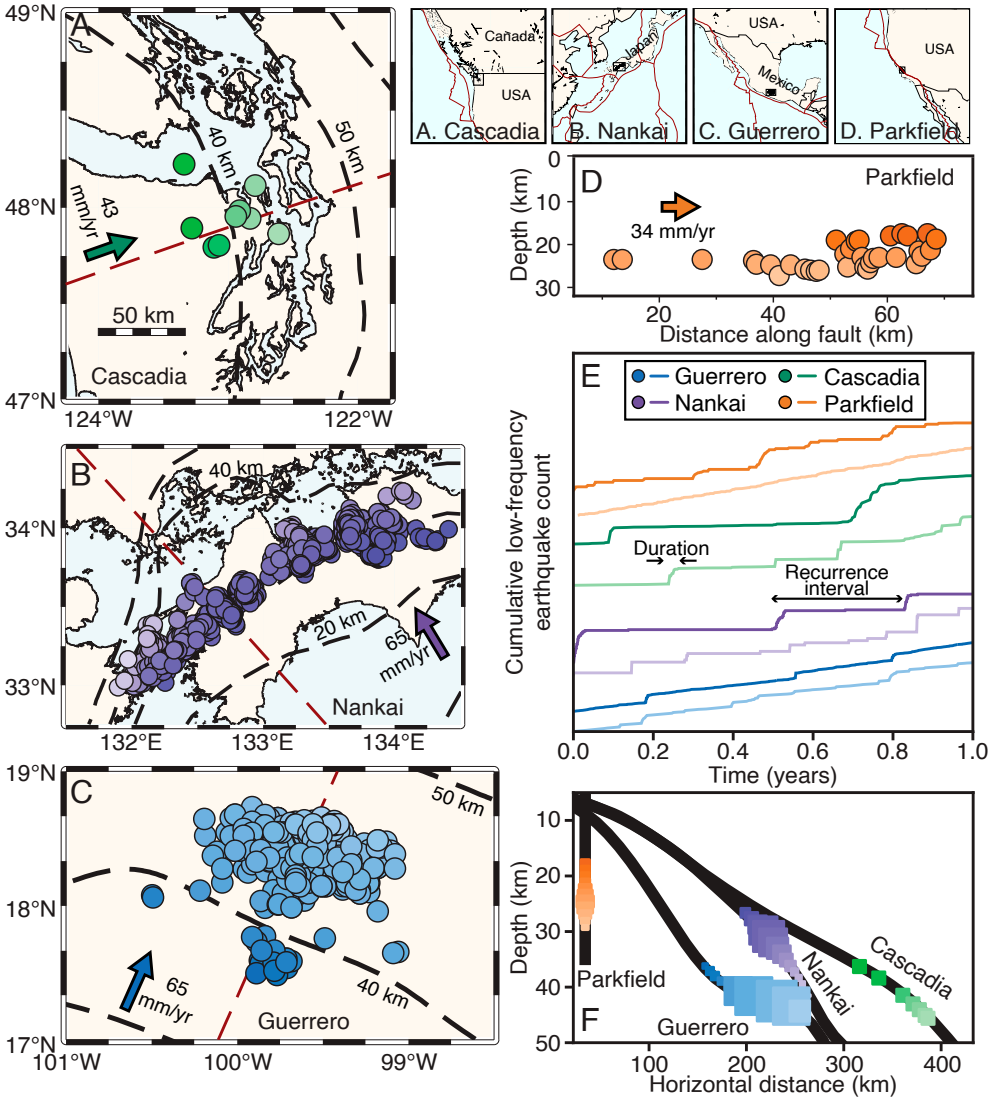

Fig. 1. Characteristic depth dependence of low-frequency earthquakes across four tectonic plate boundaries. (*A*–*D*) Colored circles represent the source locations of low-frequency earthquakes in three subduction zones (33, 37, 38)—green in (*A*) Cascadia, purple in (*B*) Nankai, and blue in (*C*) Guerrero, and orange along the (*D*) Parkfield section of the San Andreas transform plate boundary (39). The color gradient in each region shows the relative depth of the low-frequency earthquake sources, with lighter colors corresponding to deeper sources. The colored arrows in (*A*–*D*) indicate the direction and rate of tectonic motion. The dashed dark red lines show the locations of the vertical profiles of slab geometry in (*F*). *Top Right Inset* maps show the regional geographical contexts, with dark red lines showing plate boundaries and black likes showing geographical boundaries. (*E*) Cumulative event counts of two low-frequency earthquake sources from each region, one shallow (dark color) and one deep (light color) that show how shallow sources emit infrequent swarms of low-frequency earthquakes, while deep swarms occur more regularly. (*F*) Slab geometries and spatial distributions of low-frequency earthquake depth bins, shown as colored squares whose size indicates the relative number of low-frequency earthquake families in each bin. The thick black lines are the slab profiles for the three subduction zones (40, 41); Parkfield is shown as a vertical line.

depths within the transition zone, the cadence of slow slip (5, 27) and low-frequency earthquake swarms (30, 32, 36) increases. This depth-dependent transition of slow slip and low-frequency earthquake behavior from shallower, infrequent events to deeper, quasi-continuous activity appears analogous to the gradual shift from frictional slip to viscous creep we would expect within the deep transition zone.

Here we investigate the dynamics of plate boundary motion within the frictional–viscous transition zone downdip of the seismogenic zone, the source region of deep episodic slow slip. We quantify how the time scales of slow slip vary with depth by systematically measuring the durations and recurrence intervals of low-frequency earthquake swarms at three subduction zones and one transform plate boundary (Fig. 1). These time scales provide important constraints on the faulting mechanics within the transition from frictional slip to viscous creep, underscoring the first-order control of temperature on slow slip dynamics at the base of the seismogenic zone.

Depth Dependence of Low-Frequency Earthquake Dynamics

We analyze the systematics of low-frequency earthquake activity at the Nankai (37), Cascadia (33), Parkfield (39), and Guerrero (38) plate boundaries (Fig. 1). All catalogs were built with a matched-filtering approach that groups detected events into families of similar events. Each family represents a single low-frequency earthquake source location from which all of its associated events originate (24). Every regional catalog is thus made up of families that can each produce hundreds to thousands

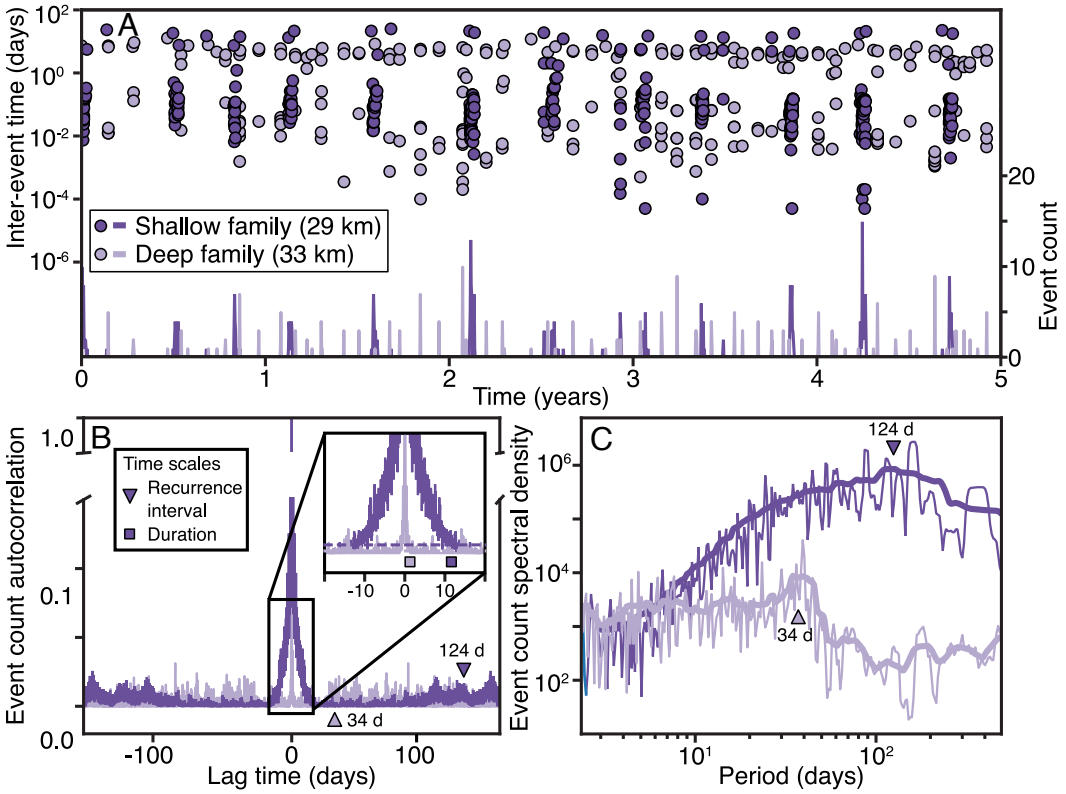

Fig. 2. Measuring the time scales of low-frequency earthquake swarms, a proxy for episodic slow slip. (*A*) Interevent times (points) and hourly event count time series (lines) of two representative low-frequency earthquake sources in Nankai. The deep source (light purple) generates event swarms more often than the shallow source (dark purple). (*B*) Autocorrelations of the two low-frequency earthquake event count time series in A. We measure the average duration *D* of low-frequency earthquake swarms as the width of the central peak of the autocorrelation. The *Inset* zoom shows an example of the systematic trend of deeper sources exhibiting shorter durations. (*C*) Fourier transform of the two low-frequency earthquake event count autocorrelation functions in (*B*). We measure the average recurrence interval *R* of the low-frequency earthquake swarms as the period of the spectral peak, as shown by the triangles.

of low-frequency earthquakes. We show representative examples of the cumulative seismic activity for updip and downdip families from each plate boundary in Fig. 1*E*. Characteristic of all regions, we see that updip sources produce infrequent and discrete bursts of activity, while swarms of events from the downdip families occur more often.

We estimate the time scales of this depth-dependent low-frequency earthquake behavior by quantifying the average recurrence and duration of the characteristic swarms of events associated with regularly recurring slow slip. We first measure the time history of every low-frequency earthquake family—each defined by a common source location on the plate boundary—by computing hourly counts of seismic activity. Each event count time series quantifies when and how every low-frequency earthquake source is active, notably capturing the event swarms that signal episodes of slow slip. In each region, we spatially group and sum the event count time series of low-frequency earthquake sources into 5-km depth bins to estimate the average seismic behavior at a given depth, assuming that sources at similar depths share similar slow slip dynamics (*SI Appendix, Materials and Methods*); we consider each of the nine families in Cascadia individually (Fig. 1*F*). We measure the duration and recurrence interval of low-frequency earthquake swarms by considering the seismic activity as a point process quantified by the event count time series (Fig. 2*A*) (42, 43). The autocorrelations of the depth-binned event count time series (Fig. 2*B*) encode the two time scales of the low-frequency earthquake swarm dynamics we seek to estimate. The width of the central peak around zero lag represents the average duration of low-frequency earthquake swarms. With increasing lag times beyond this central peak, the autocorrelation continues to lose power until a second peak emerges at a lag time equal to the average recurrence interval of low-frequency earthquake swarms. This second peak is often not obvious within the time-domain autocorrelation, so we instead measure the average recurrence interval as the peak of the amplitude spectrum of the autocorrelation (Fig. 2*C*). We estimate uncertainties for both durations and recurrence intervals in each depth bin with a jackknife approach, recomputing the event count time series by summing a random subset of low-frequency earthquake families within the depth bin (*SI Appendix, Materials and Methods*).

We observe in Fig. 3 a systematic linear decrease with depth of both the recurrence intervals and durations of low-frequency earthquake swarms in every region. The low-frequency earthquake swarms symptomatic of slow slip last from hours to about a week and recur every few days to every few months. The recurrence intervals and durations of low-frequency earthquake behavior along the Parkfield section of the San Andreas transform plate boundary are 2 to 5 times shorter than those in subduction zones (35). We show in Fig. 3*C* that the durations and recurrence intervals of slow slip at every plate boundary scale linearly with one another. While the regional linear trends can vary by up to a factor of 5 (*SI Appendix*, Table S5), a single trend across all plate boundaries can explain our observations. Extrapolating this linear relationship to the longer time scales over which GNSS data constrain slow slip, we see that geodetic estimates of slow slip durations and recurrence intervals are compatible with the observed trend (*SI Appendix*, Fig. S8*A*).

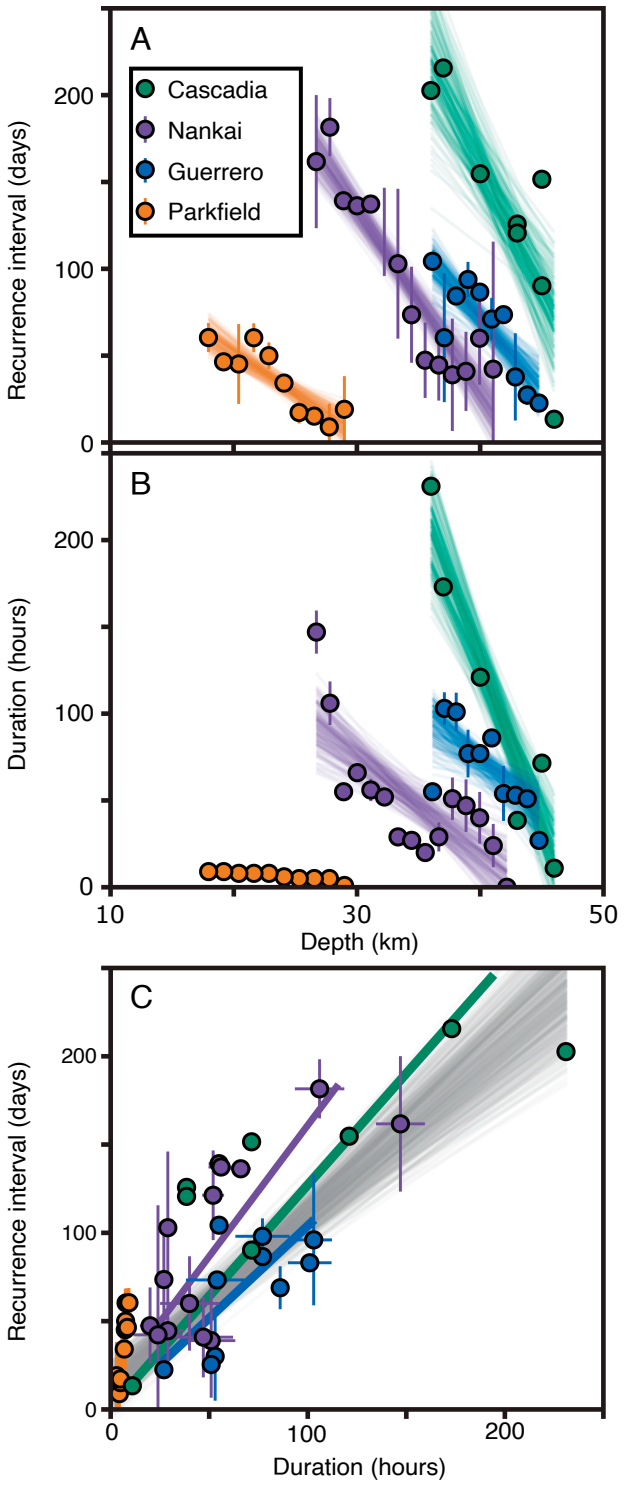

Fig. 3. Systematic decrease of the time scales of low-frequency earthquake swarms with depth. We utilize regularly recurring swarms as a proxy for slow slip. (*A*) Estimated average slow slip recurrence interval R as a function of depth. A range of linear trends is estimated by iterative resampling of the data within every depth bin. (*B*) Estimated average slow slip duration D as a function of depth. (*C*) Linear scaling of low-frequency earthquake swarm recurrence interval as a function of duration. The observed linear trends imply that the ratio R/D is constant and does not vary as a function of depth.

A Model of Episodic Slow Slip

This consistent trend of decreasing time scales of low-frequency earthquake swarms with increasing depth across multiple plate boundaries suggests common dynamics that control the timing of the slow slip that drives low-frequency earthquake activity. If we assume that the long-term fault motion of the transition zone is equal to the long-term rate of plate motion V_L and is constant with depth (44), we can then define a model of episodic fault motion to describe slow slip dynamics (35). This model supposes that the expected long-term fault motion over the recurrence interval R is entirely accommodated during an episode of slow slip of duration D. We write this model out as

$$D(z)V_S(z) = R(z)V_L, \quad [1]$$

where both slow slip time scales D and R can vary as a function of depth z, and $V_S(z)$ is the average rate of fault motion during slow slip as a function of depth z. With V_L assumed to be equal to the regional long-term rate of plate motion (Fig. 1), we can predict the slow slip rate V_S at a given depth z with estimates of the recurrence interval $R(z)$ and duration $D(z)$ of slow slip.

This model of episodic fault motion assumes that every single low-frequency earthquake occurs during regularly recurring discrete event swarms of duration D. The ratio of the duration to the recurrence interval D/R predicts the fraction of time over which all low-frequency earthquakes will occur. To evaluate how well this model describes the observed seismic activity, we calculate the episodicity e—defined as the fraction of low-frequency earthquakes whose cumulative sum of interevent times is smaller than the fraction D/R of the total catalog time—for every low-frequency earthquake family (*SI Appendix, Materials and Methods*). We observe that the large majority of families in all regions exhibit episodicities of more than 0.7 with no resolvable variation in depth (*SI Appendix*, Fig. S8). Assuming that every individual low-frequency earthquake signals slow slip, an episodicity of $e < 1$ implies that there is interepisode fault motion between the regularly recurring slow slip events that are characterized by R and D. If we incorporate interepisode slip as quantified by the episodicity e into our model, we find that the slow slip rate V_s scales with $(1 - e)$ (*SI Appendix, Materials and Methods*). The observed episodicities of >0.7 (*SI Appendix*, Fig. S8) thus imply a minor bias of up to 30% in our estimates of slow slip rate V_S. We conclude that a model of episodic faulting without interepisode slip is sufficient to explain the first-order behavior of low-frequency earthquakes.

Estimating the rate of slow slip V_S using Eq. **1**, we find a slip rate that is about 7 ± 2 mm/d and is consistent across all four plate boundaries (Fig. 4). This estimate reflects an average, combined rate of slip of both aseismic slow slip and seismic low-frequency earthquakes, even if the latter represents only a tiny fraction of the total geodetic moment (7). This average slip rate, which we predict with a simple model of episodic slow slip whose only constraint is the long-term plate motion, is compatible with typical geodetic models of slow slip (~0.1 to 1 mm/d; *SI Appendix*, Table S7).

While we assume that the long-term fault motion V_L does not vary with depth, the observed depth-independence of the slow slip rate V_S emerges from the data as the linear scaling between R and D we see in Fig. 3*C*. Eq. **1** shows how R/D effectively scales the long-term plate motion to an average slow slip rate. We can estimate a depth-independent R/D per region as the slope of the linear trends in Fig. 3*C* (*SI Appendix*, Table S5). A single best-fit slope R/D across all four plate boundaries suggests that on average slow slip rates are about 60 times faster than long-term plate motion. That the slow slip rate is roughly constant in depth and almost the same in multiple plate boundaries suggests the same mechanism controls the episodic dynamics and average rate

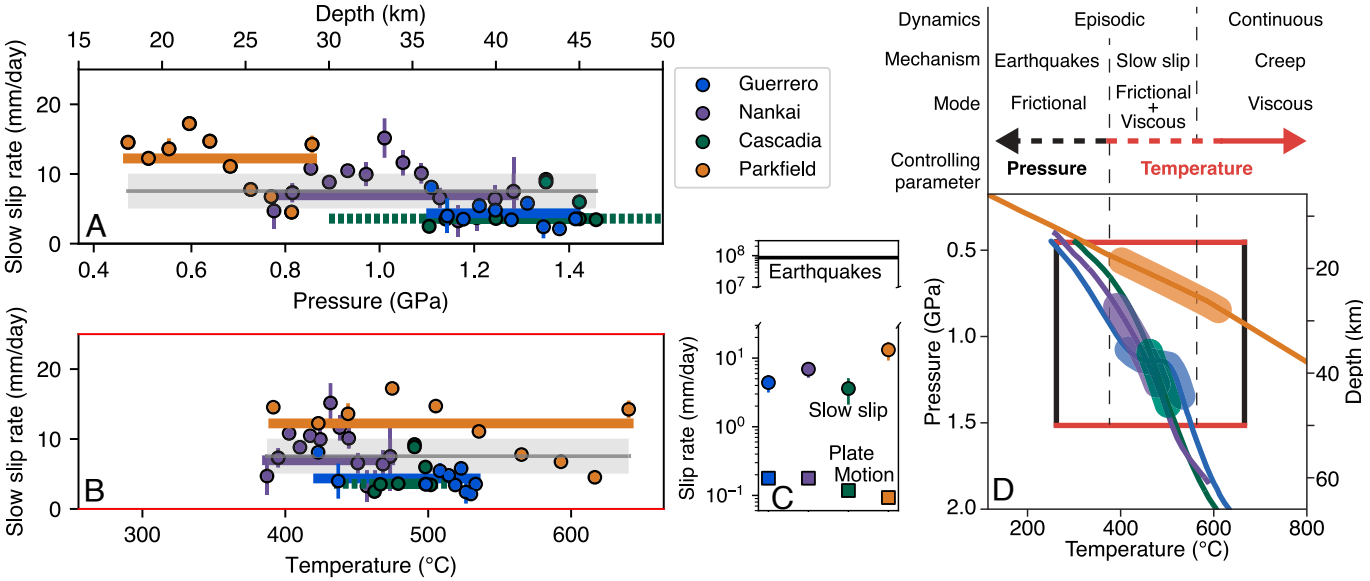

Fig. 4. Similar slow slip rate and dynamics across four plate boundaries are primarily controlled by temperature. (*A* and *B*) Slow slip rate as predicted by the model of episodic fault motion (Eq. **1**), as a function of depth and pressure (*A*) and temperature (*B*). Points represent slip rates predicted from measurements at a given depth, while bold lines show the slip rate predicted from the fitted linear trends in Fig. 3*C* whose slopes are equivalent to the ratio of time scales R/D. The dashed green line extrapolates the slow slip rate in Cascadia to the depths of the entire slow slip region (29, 44). The gray shaded region indicates the average slip rate of 7 ± 2 mm/d. We use regional thermal models to predict the temperature at the plate interface associated at a given depth and pressure (15, 45–47). The limits of pressure and temperature in A and B are set to encompass the regional thermal models, as shown by the box in D. Temperature predicts slow slip over a narrower range of values relative to pressure, with an onset of slow slip at about 400° across four plate boundaries. (*C*) Slip rates of earthquakes, slow slip, and long-term plate motion. The black horizontal curve represents an average earthquake slip rate, the points are the estimated slow slip rates, and the squares are the long-term rates of plate motion for each region. (*D*) Pressure and temperature conditions of regional thermal models and deformation regimes (15, 45–47). The box indicates the common temperature and pressure range of slow slip in *A* and *B*.

of slow slip across these varied tectonic contexts, despite their differences in geometry and lithology.

Temperature Dependence of Slow Slip Dynamics

This model of episodic fault motion does not prescribe any depth dependence of slow slip time scales and does not explain why the recurrence interval R and duration D both systematically decrease with depth (Fig. 3). If the long-term rate of fault motion V_L that loads the system is fixed, then the decrease of recurrence intervals with depth suggests that the time needed for the fault to reach failure also decreases with depth. To then maintain a depth-independent ratio of R/D (Fig. 3*C*) and slow slip rate (Fig. 4 *A* and *B*), slow slip durations must also shorten with depth. A systematic decrease in fault strength with depth would explain why deeper slow slip events become both shorter and more frequent to balance the budget of fault motion across the transition zone.

Whatever parameter controls the depth dependence of fault strength must be consistent across four plate boundaries that have different geometries, lithologies, and tectonic contexts. The primary parameters that control faulting are pressure and temperature (1). Of these two, temperature is the most likely parameter that would control fault strength downdip of the seismogenic zone. Experimental work has demonstrated that increasing temperatures weaken Earth materials (48, 49). Fault zone chemistry, including precipitation and dissolution, is also strongly dependent on temperature and can facilitate slow slip (2, 50). If we consider the depths of low-frequency earthquakes across four plate boundaries (Fig. 1*F* and *SI Appendix*, Fig. S3), pressure is an unlikely primary control on episodic slow slip dynamics. Low-frequency earthquakes in Parkfield occur at much lower confining pressures than low-frequency earthquakes in subduction zones, with source positions 10 to 20 km shallower than those in subduction zones. Another important clue is the nearly flat slab subduction of Guerrero, which demonstrates clear variations in slow slip time scales across the flat slab even as confining pressures do not vary (Fig. 1*F*). Near-lithostatic pore fluid pressures throughout the slow slip source region counteract confining pressures to lower the effective normal stress on plate boundary faults (16, 17), facilitating the existence of low-frequency earthquakes and slow slip (15, 20). To produce depth-dependent fault strength however, pore fluid pressure would have to gradually vary with depth and remain stable throughout the slow slip cycle. Geological observations and models of fault valving within the deep subduction channel suggest pore fluid pressures evolve on the time scale of individual slip events (3, 51, 52), making it unlikely that a stationary gradient in pore fluid pressure controls depth-dependent slow slip dynamics. We thus propose that temperature is the parameter that exerts a first-order control over deep slow slip dynamics across all of these tectonic contexts.

To quantitatively evaluate whether temperature better explains our observations, we return to the model of episodic fault motion (Eq. **1**). The depth-independent rate of slow slip we observe across four different plate boundaries spans a wide range of depths and pressures, more than 30 km and 1,000 MPa respectively (Fig. 4*D*). If temperature is a better predictor of where slow slip occurs along the plate boundary, our measurements of slow slip rate should span a relatively smaller range in temperature. We translate the depth of our measurements of slow slip rate to temperature via thermal models of each plate boundary (15, 45, 46). This allows us to plot our estimates of the average slow slip rate as a function of the temperatures that correspond to the range of pressures and depths of the plate interfaces in Fig. 4*B*;

we extrapolate the slow slip rate in Cascadia to a wider range of pressures and temperatures because the low-frequency earthquake catalog we analyze here (33) does not encompass the entire slow slip source region (29, 44).

We observe that our measurements across all regions are more coherent as a function of temperature rather than as a function of pressure. Once we convert the inferred source pressures, we see that low-frequency earthquakes in Parkfield occupy the same temperature space as the three subduction zones. While low-frequency earthquakes in Nankai and Cascadia span more than double the pressure range of low-frequency earthquakes in Guerrero, all three regions host this seismic activity over similar temperature ranges of about 100 °C. The onset of low-frequency earthquake activity across all four plate boundaries is consistently about 400 °C (Fig. 4*B*), despite the epistemic variability of thermal models (53). Low-frequency earthquakes then disappear in all three subduction zones beyond 550 °C; only the deepest low-frequency earthquake swarms in Parkfield occur at higher temperatures, extending up to 650 °C due to a larger geotherm (15, 54). This temperature band of 400 to 550 °C is consistent with temperatures estimated from geological observations of slow slip deformation in exhumed subduction material (2, 4). Compared to the wide spread of observed pressures over 1000 MPa, the relatively narrower, common temperature range of ∼150 °C and a similar onset of low-frequency earthquake activity around 400 °C suggest the mechanism that controls the depth dependence of deep slow slip time scales at all four plate boundaries is primarily dependent on temperature.

Slow Slip Results from the Episodic Interplay of Frictional and Viscous Deformation

The dynamics of deep slow slip reflect the dominant mode of deformation within the transition zone between the shallow seismogenic zone and creep at depth. Earthquakes at shallow depths reflect episodic frictional sliding whose failure process is principally controlled by pressure (1). Conversely, viscous creep at depth occurs quasi-continuously and its strain rate is strongly dependent on temperature (55). Our observations of episodic slow slip dynamics whose time scales appear to primarily depend on temperature point to an intermediate mode of deformation within the deep frictional–viscous transition zone that exhibits characteristics of both end-member regimes (Fig. 4*D*): the stick–slip dynamics of frictional sliding and the temperature dependence of viscous creep. If we extrapolate the trend of systematically decreasing slow slip durations and recurrence intervals with increasing depth and temperature (Fig. 3), slip will become continuous when these two time scales approach 0 (29, 35). This is consistent with slow slip deformation gradually transitioning from an episodic frictional regime to a quasi-continuous viscous one (56).

Such an interplay of frictional and viscous deformation is corroborated by the geological record of exhumed outcrops of deep plate boundaries (2–4, 57). Observations of frictional features embedded within a matrix of viscously deformed material suggest that multiple mechanisms operating in tandem are likely responsible for the characteristic kinematics of slow slip (2, 3). Another common geological observation in these settings is the signature of hydrofracturing and crack-seal veins (57, 58), suggesting the prevalence of fluids and localized low effective pressures along plate boundary faults. High pore fluid pressures within the deep transition zone are key to explain both the existence and mechanics of deep slow slip (12, 15, 52), but it is not obvious how the presence of fluids explains the depth evolution of slow slip time scales we observe here. Fluids are principally sourced from the metamorphic dehydration of the subducting oceanic lithosphere at depths beyond the seismogenic zone (4), as evinced by serpentinization of the mantle wedge (59). Even in a continental transform setting like Parkfield, temperature-sensitive metamorphic facies may act as a fluid source (17, 54, 60). Both ecologitization and serpentinization are relatively insensitive to pressure, being instead strongly dependent on temperature with an onset around 400 °C (47, 59, 61). This corresponds well with the observed onset of low-frequency earthquake activity across three subduction zones (Fig. 4*B*). We thus suggest that temperature-sensitive metamorphism plays an important role in setting the scene for the mixed-mode deformation responsible for slow slip, but does not explain the observed evolution of slow slip time scales with depth (Fig. 3).

Our observations of episodic slow slip time scales place robust geophysical constraints on the dynamics of the mixed-mode deformation responsible for slow slip within the deep transition zone. Any mechanism responsible for deep slow slip must produce the temperature-dependent episodic dynamics that we observe here across four plate boundaries. Recent models of slow slip have included a temperature-dependent viscous component that deforms quasi-continuously, both between and during slow slip events (19, 20, 62–64). As temperature increases, a weaker viscous matrix would creep faster and accommodate a larger majority of the total deformation, keeping stresses low and stifling the build-up of elastic strain energy needed for the cyclic frictional failure that produces the observed episodic slip dynamics. This effectively increases slow slip recurrence intervals as temperatures rise, which does not fit our observations (Fig. 3*A*).

The characteristic episodic behavior of slow slip that we observe here suggests that there must be little to no fault motion between discrete episodes of slow slip (25, 28, 65). This implies that relatively strong heterogeneities within the subduction channel must jam the shear zone and inhibit viscous shear while elastic stresses build prior to the next slow slip event (57, 63). This also suggests that these same heterogeneities must prevent the viscous material from being interconnected, otherwise it would flow continuously as the weakest material in the shear zone; an interconnected viscous matrix is likely a requisite feature to complete the transition to continuous creep at depth. Once the yield stress is reached and slow slip nucleates, the viscous material would then control the temperature-dependent response of the shear zone to the frictional failure (64). This explains the systematic decrease in slow slip duration with depth (Fig. 3*B*), as increasing temperatures will weaken the viscous material and reduce relaxation time scales. If there is no viscous creep in between slow slip episodes, then the recurrence interval of slow slip must uniquely depend on the frictional properties of the strong heterogeneities that jam the shear zone (62). Experimental work has demonstrated the temperature dependence of friction (48), with higher temperatures leading to failure at relatively lower stresses (66). This implies shorter slow slip recurrence intervals at greater depths and temperatures, consistent with our observations. We thus suggest that increasing temperatures with depth can explain the systematic decrease of both time scales of the episodic dynamics of slow slip in the deep transition zone.

Our observations of a constant slow slip rate across four different plate boundaries (Fig. 4) have implications for how we measure slow slip and understand its physics. The moment M_0 of

any given slow slip event measured here is $M_0 = \mu V_S DA$, where μ is the shear modulus, V_S is the slow slip rate, D is the slipping duration, and A is the slipping area. Following our observations of a V_S that is constant and independent of depth (Fig. 4), our results suggest that the slow slip moment M_0 only varies with A and D. If we assume that A scales with D^2 like a typical earthquake (67)—a relation that our results do not directly constrain—our observations of a constant V_S could imply an earthquake-like cubic moment-duration scaling for slow slip (22); this would not be consistent with past work that supports a linear scaling of slow slip moment M_0 to duration D (68). The constant slow slip rate V_S we observe here is however inconsistent with recent work that demonstrates that the moment rates of both slow slip and low-frequency earthquakes covary throughout the slow slip cycle (22, 28, 69, 70). These contradictory observations highlight the challenge in placing robust constraints on the physics of slow slip, often complicated by the broad range of temporal and spatial scales over which geophysical measurements are made. Our observations here represent slow slip dynamics averaged over many events in time; the rapid recurrence intervals in Parkfield imply the slow slip time scales measured here were averaged over more than 1,000 slip cycles. The slow slip time scales we estimated also reflect a spatial average across the along-strike extent of the slow slip source region because we bin low-frequency earthquake activity as a function of depth. Our estimates of the duration and recurrence of slow slip thus represent an average behavior that is in reality more complex than the periodic slip transients assumed by our model of episodic fault motion. Averaging over many slow slip cycles acts as a low-pass filter, hiding both variations in slow slip moment rates that only appear at daily or even subdaily time scales (22, 25–28, 69–71) and kilometer-scale heterogeneities on the plate interface that can only be identified with precise low-frequency earthquake locations (72). This highlights that even as we are able to capture the gross systematics of slow slip across multiple plate boundaries, further work at such short time and spatial scales is necessary to further constrain the mechanism of frictional–viscous interplay responsible for slow slip.

Data, Materials, and Software Availability. The low-frequency earthquake catalogs that we analyzed here are publicly available. The Guerrero, Parkfield, and Nankai catalogs are available from the Slow Earthquake Database (ref. 73); the Cascadia catalog is available as supplementary material for ref. 33.

ACKNOWLEDGMENTS. We thank Benjamin Malvoisin, Gaspard Farge, Camilla Cattania, Matěj Peč, Jared Bryan, and Roland Bürgmann for discussions that improved this manuscript. Z.E.Y. and M.R. acknowledge the Université Grenoble Alpes for supporting this work through the IDEX International Mobility Fund. B.R., M.R., and W.B.F. acknowledge the Centre National de Recherche Scientifique (CNRS) for supporting this work through the International Research Project SlowFaults. B.R., M.R., and W.B.F. acknowledge the Massachusetts Institute of Technology (MIT) for supporting the work through the MIT International Science and Technology Initiatives (MISTI) Global Seed Fund and the MIT-France Seed Fund. M.R. acknowledges the Agence Nationale de la Recherche (ANR) for supporting this work through the project (ANR-21-CE49-0023).

Author affiliations: [a]Institut des Sciences de La Terre (ISTerre), Univ. Grenoble Alpes, Univ. Savoie Mont Blanc, CNRS, Institut de recherche pour le développement, Univ. Gustave Eiffel, Grenoble 38000, France; [b]Institut Terre & Environnement de Strasbourg, Université de Strasbourg, Strasbourg 67084, France; and [c]Department of Earth, Atmospheric and Planetary Sciences, Massachusetts Institute of Technology, Cambridge, MA 02139

1. C. H. Scholz, Earthquakes and friction laws. *Nature* **391**, 37–42 (1998).
2. Å. Fagereng, G. W. Hillary, J. F. Diener, Brittle-viscous deformation, slow slip, and tremor. *Geophys. Res. Lett.* **41**, 4159–4167 (2014).
3. K. Ujiie *et al.*, An explanation of episodic tremor and slow slip constrained by crack-seal veins and viscous shear in subduction mélange. *Geophys. Res. Lett.* **45**, 5371–5379 (2018).
4. W. M. Behr, R. Bürgmann, What's down there? the structures, materials and environment of deep-seated slow slip and tremor *Philos. Trans. R. Soc. A Math. Phys. Eng. Sci.* **379**, 20200218 (2021).
5. T. Nishimura, T. Matsuzawa, K. Obara, Detection of short-term slow slip events along the Nankai trough, southwest Japan, using GNSS data. *J. Geophys. Res. Solid Earth* **118**, 3112–3125 (2013).
6. H. Dragert, K. Wang, T. S. James, A silent slip event on the deeper Cascadia subduction interface. *Science* **292**, 1525–1528 (2001).
7. V. Kostoglodov *et al.*, The 2006 slow slip event and nonvolcanic tremor in the Mexican subduction zone. *Geophys. Res. Lett.* **37**, e2010GL045424 (2010).
8. L. M. Wallace, Slow slip events in New Zealand. *Annu. Rev. Earth Planet. Sci.* **48**, 175–203 (2020).
9. B. Rousset, R. Bürgmann, M. Campillo, Slow slip events in the roots of the San Andreas fault. *Sci. Adv.* **5**, aav3274 (2019).
10. R. Bilham *et al.*, Surface creep on the north Anatolian fault at ismetpasa, turkey, 1944–2016. *J. Geophys. Res. Solid Earth* **121**, 7409–7431 (2016).
11. E. Neyrinck *et al.*, The slow slip event cycle along the Izmit segment of the north Anatolian fault. *Earth Planet. Sci. Lett.* **648**, 119104 (2024).
12. R. Bürgmann, The geophysics, geology and mechanics of slow fault slip. *Earth Planet. Sci. Lett.* **495**, 112–134 (2018).
13. L. M. Wallace *et al.*, Slow slip near the trench at the hikurangi subduction zone, New Zealand. *Science* **352**, 701–704 (2016).
14. E. Araki *et al.*, Recurring and triggered slow-slip events near the trench at the Nankai trough subduction megathrust. *Science* **356**, 1157–1160 (2017).
15. X. Gao, K. Wang, Rheological separation of the megathrust seismogenic zone and episodic tremor and slip. *Nature* **543**, 416–419 (2017).
16. P. Audet, M. G. Bostock, N. I. Christensen, S. M. Peacock, Seismic evidence for overpressured subducted oceanic crust and megathrust fault sealing. *Nature* **457**, 76–78 (2009).
17. A. M. Thomas, R. M. Nadeau, R. Bürgmann, Tremor-tide correlations and near-lithostatic pore pressure on the deep San Andreas fault. *Nature* **462**, 1048–1051 (2009).
18. P. Segall, A. M. Rubin, A. M. Bradley, J. R. Rice, Dilatant strengthening as a mechanism for slow slip events. *J. Geophys. Res. Solid Earth* **115**, e2010JB007449 (2010).
19. A. Goswami, S. Barbot, Slow-slip events in semi-brittle serpentinite fault zones. *Sci. Rep.* **8**, 6181 (2018).
20. W. M. Behr, T. V. Gerya, C. Cannizzaro, R. Blass, Transient slow slip characteristics of frictional-viscous subduction megathrust shear zones. *AGU Adv.* **2**, e2021AV000416 (2021).
21. W. B. Frank, Slow slip hidden in the noise: The intermittence of tectonic release. *Geophys. Res. Lett.* **43**, 10125–10133 (2016).
22. W. B. Frank, E. E. Brodsky, Daily measurement of slow slip from low-frequency earthquakes is consistent with ordinary earthquake scaling. *Sci. Adv.* **5**, eaaw9386 (2019).
23. D. R. Shelly, G. C. Beroza, S. Ide, S. Nakamula, Low-frequency earthquakes in shikoku, Japan, and their relationship to episodic tremor and slip. *Nature* **442**, 188–191 (2006).
24. S. Chestler, K. Creager, A model for low-frequency earthquake slip. *Geochem. Geophys. Geosyst.* **18**, 4690–4708 (2017).
25. W. B. Frank, B. Rousset, C. Lasserre, M. Campillo, Revealing the cluster of slow transients behind a large slow slip event. *Sci. Adv.* **4**, eaat0661 (2018).
26. B. Rousset, Y. Fu, N. Bartlow, R. Bürgmann, Weeks-long and years-long slow slip and tectonic tremor episodes on the south central Alaska megathrust. *J. Geophys. Res. Solid Earth* **124**, 13392–13403 (2019).
27. Z. El Yousfi *et al.*, Intermittence of transient slow slip in the Mexican subduction zone. *Earth Planet. Sci. Lett.* **620**, 118340 (2023).
28. C. Mouchon, W. B. Frank, M. Radiguet, P. Poli, N. Cotte, Subdaily slow fault slip dynamics captured by low-frequency earthquakes. *AGU Adv.* **4**, e2022AV000848 (2023).
29. A. G. Wech, K. C. Creager, A continuum of stress, strength and slip in the Cascadia subduction zone. *Nat. Geosci.* **4**, 624–628 (2011).
30. D. R. Shelly, K. M. Johnson, Tremor reveals stress shadowing, deep postseismic creep, and depth-dependent slip recurrence on the lower-crustal San Andreas fault near Parkfield. *Geophys. Res. Lett.* **38**, e2011GL047863 (2011).
31. K. Obara, S. Tanaka, T. Maeda, T. Matsuzawa, Depth-dependent activity of non-volcanic tremor in southwest Japan. *Geophys. Res. Lett.* **37**, e2010GL043679 (2010).
32. W. Frank *et al.*, Along-fault pore-pressure evolution during a slow-slip event in Guerrero, Mexico. *Earth Planet. Sci. Lett.* **413**, 135–143 (2015).
33. J. R. Sweet, K. C. Creager, H. Houston, S. R. Chestler, Variations in Cascadia low-frequency earthquake behavior with downdip distance. *Geochem. Geophys. Geosyst.* **20**, 1202–1217 (2019).
34. W. B. Frank *et al.*, Uncovering the geodetic signature of silent slip through repeating earthquakes. *Geophys. Res. Lett.* **42**, 2774–2779 (2015).
35. A. M. Thomas, N. M. Beeler, Q. Bletery, R. Burgmann, D. R. Shelly, Using low-frequency earthquake families on the San Andreas fault as deep creepmeters. *J. Geophys. Res. Solid Earth* **123**, 457–475 (2018).
36. K. Obara, Characteristics and interactions between non-volcanic tremor and related slow earthquakes in the Nankai subduction zone, southwest Japan. *J. Geodyn.* **52**, 229–248 (2011).
37. A. Kato, S. Nakagawa, Detection of deep low-frequency earthquakes in the Nankai subduction zone over 11 years using a matched filter technique. *Earth Planets Space* **72**, 128 (2020).
38. W. B. Frank *et al.*, Using systematically characterized low-frequency earthquakes as a fault probe in Guerrero, Mexico. *J. Geophys. Res. Solid Earth* **119**, 7686–7700 (2014).
39. D. R. Shelly, A 15 year catalog of more than 1 million low-frequency earthquakes: Tracking tremor and slip along the deep San Andreas fault. *J. Geophys. Res. Solid Earth* **122**, 3739–3753 (2017).
40. G. P. Hayes *et al.*, Slab2, a comprehensive subduction zone geometry model. *Science* **362**, 58–61 (2018).
41. F. Hirose, J. Nakajima, A. Hasegawa, Three-dimensional seismic velocity structure and configuration of the Philippine sea slab in southwestern Japan estimated by double-difference tomography. *J. Geophys. Res. Solid Earth* **113**, e2007JB005274 (2008).

42. S. B. Lowen, M. C. Teich, *Fractal-Based Point Processes* (Wiley Online Library, 2005).
43. W. B. Frank *et al*., The evolving interaction of low-frequency earthquakes during transient slip. *Sci. Adv.* **2**, e1501616 (2016).
44. N. M. Bartlow, A long-term view of episodic tremor and slip in Cascadia. *Geophys. Res. Lett.* **47**, e2019GL085303 (2020).
45. S. M. Peacock, Thermal and metamorphic environment of subduction zone episodic tremor and slip. *J. Geophys. Res. Solid Earth* **114**, e2008JB005978 (2009).
46. P. E. van Keken, I. Wada, G. A. Abers, B. R. Hacker, K. Wang, Mafic high-pressure rocks are preferentially exhumed from warm subduction settings. *Geochem. Geophys. Geosyst.* **19**, 2934–2961 (2018).
47. C. B. Condit, V. E. Guevara, J. R. Delph, M. E. French, Slab dehydration in warm subduction zones at depths of episodic slip and tremor. *Earth Planet. Sci. Lett.* **552**, 116601 (2020).
48. M. L. Blanpied, D. A. Lockner, J. D. Byerlee, Frictional slip of granite at hydrothermal conditions. *J. Geophys. Res. Solid Earth* **100**, 13045–13064 (1995).
49. Si. Karato, *Deformation of Earth Materials: An Introduction to the Rheology of Solid Earth* (Cambridge University Press, 2008).
50. P. Audet, R. Bürgmann, Possible control of subduction zone slow-earthquake periodicity by silica enrichment. *Nature* **510**, 389–392 (2014).
51. S. Taetz, T. John, M. Bröcker, C. Spandler, A. Stracke, Fast intraslab fluid-flow events linked to pulses of high pore fluid pressure at the subducted plate interface. *Earth Planet. Sci. Lett.* **482**, 33–43 (2018).
52. S. Ozawa, Y. Yang, E. M. Dunham, Fault-valve instability: A mechanism for slow slip events. *J. Geophys. Res. Solid Earth* **129**, e2024JB029165 (2024).
53. G. M. Hobson, D. A. May, Sensitivity analysis of the thermal structure within subduction zones using reduced-order modeling. *Geochem. Geophys. Geosyst.* **26**, e2024GC011937 (2025).
54. A. Fagereng, J. F. A. Diener, San Andreas fault tremor and retrograde metamorphism. *Geophys. Res. Lett.* **38**, e2011GL049550 (2011).
55. G. Hirth, J. Tullis, Dislocation creep regimes in quartz aggregates. *J. Struct. Geol.* **14**, 145–159 (1992).
56. Å. Fagereng, A. Beall, Is complex fault zone behaviour a reflection of rheological heterogeneity? *Philos. Trans. R. Soc. A* **379**, 20190421 (2021).
57. Å. Fagereng, S. A. Den Hartog, Subduction megathrust creep governed by pressure solution and frictional-viscous flow. *Nat. Geosci.* **10**, 51–57 (2017).
58. J. P. Platt, D. Grujic, N. J. Phillips, S. Piazolo, D. A. Schmidt, Geological fingerprints of deep slow earthquakes: A review of field constraints and directions for future research. *Geosphere* **20**, 981–1004 (2024).
59. E. Legros *et al*., Massive mg-rich fluid release across the brucite + serpentine reaction in subduction zones. *Earth Planet. Sci. Lett.* **671**, 119602 (2025).
60. P. M. Fulton, D. M. Saffer, B. A. Bekins, A critical evaluation of crustal dehydration as the cause of an overpressured and weak San Andreas fault. *Earth Planet. Sci. Lett.* **284**, 447–454 (2009).
61. B. R. Hacker, G. A. Abers, S. M. Peacock, Subduction factory 1. Theoretical mineralogy, densities, seismic wave speeds, and h2o contents. *J. Geophys. Res. Solid Earth* **108**, e2001JB001127 (2003).
62. E. G. Daub, D. R. Shelly, R. A. Guyer, P. A. Johnson, Brittle and ductile friction and the physics of tectonic tremor. *Geophys. Res. Lett.* **38**, e2011GL046866 (2011).
63. A. Beall, Å. Fagereng, S. Ellis, Fracture and weakening of jammed subduction shear zones, leading to the generation of slow slip events. *Geochem. Geophys. Geosyst.* **20**, 4869–4884 (2019).
64. R. Ando, K. Ujiie, N. Nishiyama, Y. Mori, Depth-dependent slow earthquakes controlled by temperature dependence of brittle-ductile transitional rheology. *Geophys. Res. Lett.* **50**, e2022GL101388 (2023).
65. R. Jolivet, W. B. Frank, The transient and intermittent nature of slow slip. *AGU Adv.* **1**, e2019AV000126 (2020).
66. S. Barbot, A rate-, state-, and temperature-dependent friction law with competing healing mechanisms. *J. Geophys. Res. Solid Earth* **127**, e2022JB025106 (2022).
67. H. Kanamori, E. E. Brodsky, The physics of earthquakes. *Rep. Progr. Phys.* **67**, 1429 (2004).
68. S. Ide, G. C. Beroza, Slow earthquake scaling reconsidered as a boundary between distinct modes of rupture propagation. *Proc. Natl. Acad. Sci. U.S.A.* **120**, e2222102120 (2023).
69. J. C. Hawthorne, A. M. Rubin, Short-time scale correlation between slow slip and tremor in Cascadia. *J. Geophys. Res. Solid Earth* **118**, 1316–1329 (2013).
70. Y. Itoh, A. Socquet, M. Radiguet, Slip-tremor interaction at the very beginning of episodic tremor and slip in Cascadia. *AGU Adv.* **6**, e2024AV001425 (2025).
71. B. Gombert, J. C. Hawthorne, Rapid tremor migration during few minute-longs low earth-614 quakes in Cascadia. *J. Geophys. Res. Solid Earth* **128**, e2022JB025034 (2023).
72. A. M. Rubin, J. G. Armbruster, Imaging slow slip fronts in Cascadia with high precision cross-station tremor locations. *Geochem. Geophys. Geosyst.* **14**, 5371–5392 (2013).
73. M. Kano *et al*., Development of a slow earthquake database. *Seismol. Res. Lett.* **89**, 1566–1575 (2018).